An improved post-processing method and an analysis of wideband channel sounding results

Chia Leong Hong

Technical report
CUED/F-INFENG/TR.477

Laboratory for Communications Engineering
Department of Engineering
University of Cambridge

6 November 2001

Abstract
This report summarises the work done during the period from 1 October 2001 to 5 November 2001. A post-processing method for extracting the power delay profiles and RMS delay spread from wideband channel sounding data is described, along with preliminary results on the statistics of RMS delay spread. The results show that RMS delay spread is highly correlated to the excess path loss. Further measurements are necessary to quantify the effect of antenna height and distance on RMS delay spread.

1 Introduction

In the draft first year report [1], an overview of channel parameters frequently used to characterise a wideband radio channel has been presented. It was shown that the dispersion of the channel can be represented by the use of power delay profile. One relevant parameter is the *root mean squared delay spread*, τ_{RMS}, which is the second central moment of the power delay profile. However RMS delay spread is not an infallible way of characterising the radio channel. It is widely noted that τ_{RMS} is very sensitive to noise components having large excess delays [2]. In fact, not all channel sounders have the same dynamic range and sensitivity, thus it was recommended in [2] that along with the delay spread, one should report the noise exclusion threshold used during the processing of the data. In this report, a method based on correlation processing is used to improve the dynamic range of the measured results. This technique is reported along with an analysis of the effect of the noise threshold on the RMS delay spread of the processed data.

2 Methods

2.1 Theory

The radio channel is often modelled as a linear time-variant filter with impulse response $h(t,\tau)$ or equivalently by its frequency response $H(f,t)$, where $h(t,\tau)$ and $H(f,t)$ are a Fourier transform pair [3]. Without loss of generality, consider a linear time-invariant system that is characterised by its impulse response $h(\tau)$, as shown in Figure 2.1.

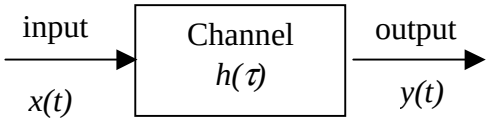

Figure 2.1 Linear single input/single output system

The complex envelope of the channel output $y(t)$ is the convolution of the impulse response $h(\tau)$ with the complex envelope of the channel input $x(t)$, i.e.

$$y(t) = x(t) \otimes h(\tau) = \int_{-\infty}^{\infty} h(\tau) x(t-\tau) d\tau \tag{1}$$

The time-invariant impulse response $h(\tau)$ is a special case of the time-variant impulse response $h(t,\tau)$ if the unit impulse response function is independent on the time an input is applied, i.e.,

$$h(t,\tau) = h(\tau) \quad \text{for } -\infty < t < \infty \tag{2}$$

To estimate the channel impulse response $h(\tau)$, a first step is to cross-correlate the input of the channel with its output, assuming that the input to the channel, i.e. the transmitted signal, is known. For jointly stationary stochastic processes $x(t)$ and $y(t)$, it can be shown [4] that their cross-correlation $\phi_{xy}(\tau)$ is related to the autocorrelation of the input $\phi_{xx}(\tau)$ as

$$\phi_{xy}(\tau) = \int_{-\infty}^{\infty} h(\alpha) \phi_{xx}(\tau - \alpha) d\alpha \tag{3}$$

which is a convolution integral. Since convolution in time domain is equivalent to multiplication in frequency domain, the relation (3) becomes

$$\Phi_{xy}(f) = \Phi_{xx}(f) H(f) \tag{4}$$

where $\Phi_{xy}(f)$ denotes the Fourier transform of $\phi_{xy}(\tau)$, $\Phi_{xx}(f)$ denotes the Fourier transform of $\phi_{xx}(\tau)$ and $H(f)$ is the frequency response of the channel. $\Phi(f)$ is also known as the *power density spectrum* or the *spectral density* of a stochastic process.

Hence, the channel impulse response $h(\tau)$ is found via the inverse Fourier transform of its frequency response $H(f)$. Thus we may write

$$h(\tau) = \Im^{-1}[H(f)] = \Im^{-1}\left[\frac{\Im[\phi_{xy}(\tau)]}{\Im[\phi_{xx}(\tau)]}\right] \quad (5)$$

where $\Im^{-1}$ denotes the inverse Fourier transform and $\Im$ denotes the forward Fourier transform.

Equation (5) forms the basis of the technique used in the post-processing algorithm.

2.2 Post-processing Algorithm

Given the transmitted channel sounding sequence, and the received signal, the channel impulse response can be calculated using the following method:

1. find $\phi_{xx}(\tau)$, the autocorrelation of the transmitted sequence
2. find $\phi_{xy}(\tau)$, the cross-correlation of the received signal with the transmitted signal
3. Fourier transform the correlation functions to give $\Phi_{xy}(f)$ and $\Phi_{xx}(f)$.
4. divide $\Phi_{xy}(f)$ by $\Phi_{xx}(f)$ to give $H(f)$.
5. apply the inverse Fourier transform to $H(f)$ to give $h(\tau)$.
6. Evaluate the power delay profile which is the average of the magnitude squared of $h(\tau)$, $P(\tau) = \frac{E[|h(\tau)|^2]}{2}$
7. calculate the RMS delay spread according to $\tau_{RMS} = \sqrt{\frac{1}{P}\sum_{i=1}^{n} P_i \tau_i^2 - \tau_0^2}$ where $\tau_0 = \frac{1}{P}\sum_{i=1}^{n} P_i \tau_i$.

Note that the received signal $y(t)$ is subject to distortion owing to the gain and phase imbalance present in the quadrature demodulator. It is necessary to eliminate this error prior to further processing. The algorithm *remove_squint* is called to reduce phase and gain imbalance from the received signal prior to the subsequent correlation processing.

2.3 Dynamic range enhancement

The application of the Discrete Fourier transform (DFT) brings with it an inherent assumption that the input signal is periodic with respect to the transform block,

otherwise the result of the DFT will be affected by “spectral leakage”, which is caused when a discontinuity in the time domain waveform is translated into frequency domain spectral spreading or *leakage*. This cannot be guaranteed in the processing of the correlation signals which can be viewed as truncated waveform blocks. One way to overcome this characteristic of the DFT is to use a *window function* prior to transform processing. It is a common practice to use a window function to *taper* the original signal before DFT transformation [5]. The window function serves to reduce discontinuity at both edges of the original signal. In this case the window function is multiplied with the correlation waveforms before applying the DFT. There are many choices of window function; the ones which are investigated here are the Hamming, Hanning and Blackman window. These window functions are selected based on the width of the main lobe and low sidelobe levels. The length of the window is also a matter for consideration. The next section illustrates the effect of the window function and the window size on the power delay profile and the RMS delay spread.

3 Results

3.1 Effect of Window function and window length on Power Delay Profile

Figure 3.1 shows a typical power delay profile obtained from maximum-likelihood processing using 10 estimated channel response measurements. The Y-axis is plotted using a dB scale, and is shifted upward by 30dB. From Figure 3.1, it can be seen that the noise floor is about 20dB below peak response.

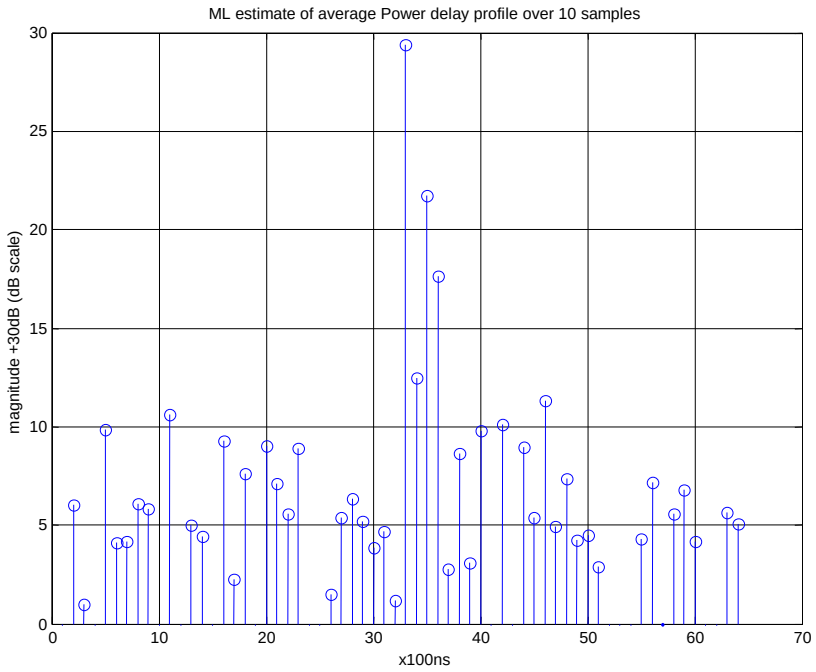

Figure 3.1 Maximum Likelihood estimate of Power Delay Profile

Figure 3.2 shows the result of correlation processing, with a rectangular window function and a DFT block length of 254 samples, from one channel estimate. The Power Delay Profile (PDP) shows little noise compared to the maximum-likelihood method. The majority of noise has been eliminated. However, some spurious noise introduced by the FFT processing with rectangular windowing remains less than 30dB down on the peak value. The frequency response plot also shows a somewhat peaky characteristic.

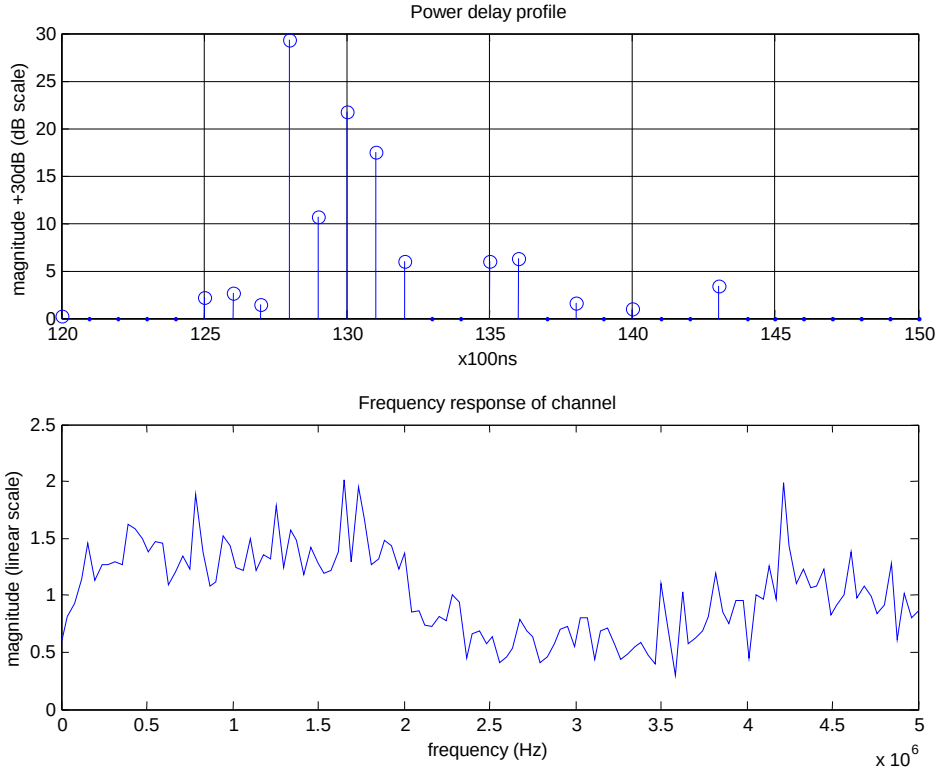

Figure 3.2 Power Delay Profile and frequency response with rectangular windowing

Figure 3.3 shows the effect of applying a Hamming window on the same delay profile with the same block length. While the frequency response has been smoothed due to windowing, the delay profile is now virtually noise free at a level 30dB below the peak value.

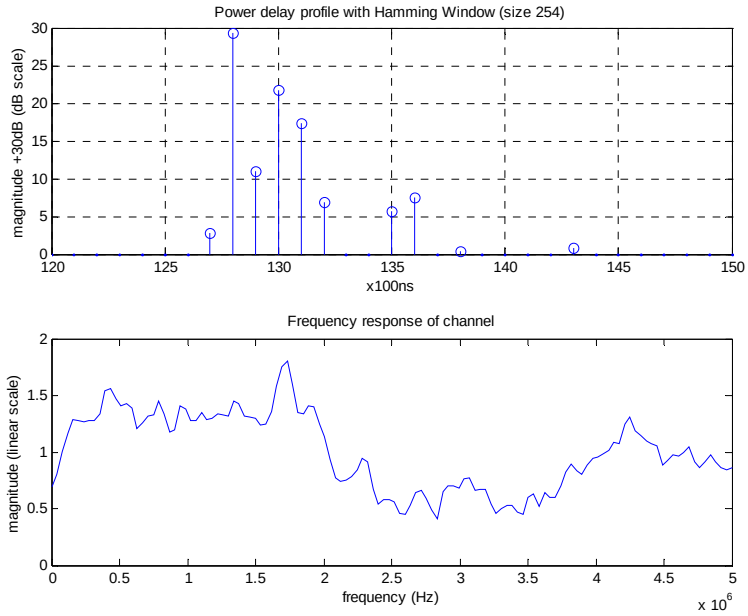

Figure 3.3 Power Delay Profile and frequency response with a Hamming Window (length 254 samples)

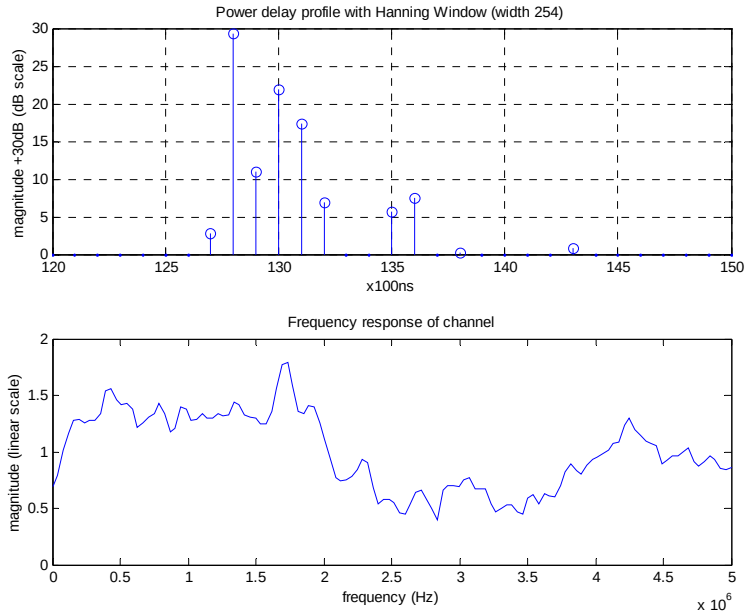

Figure 3.4 Power Delay Profile and frequency response with a Hanning Window (length 254 samples)

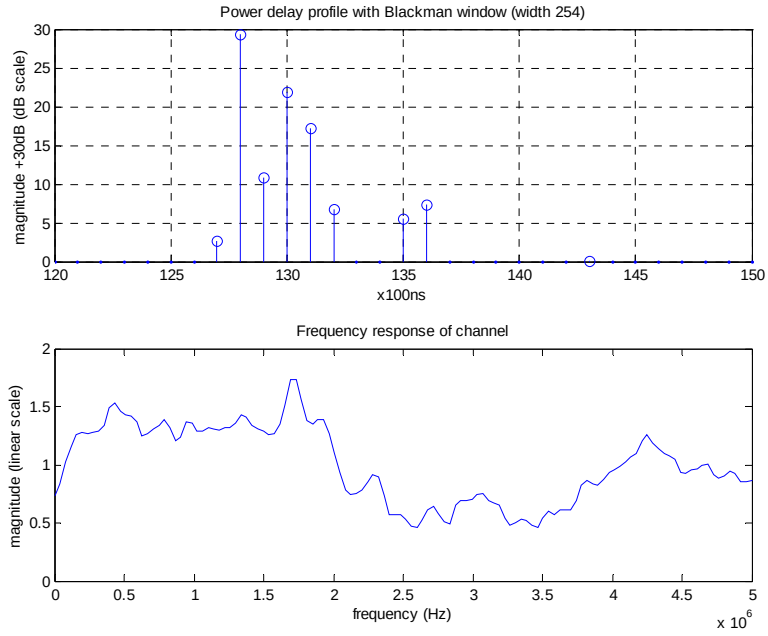

Figure 3.5 Power Delay Profile and frequency response with a Blackman Window (length 254 samples)

Figure 3.4 shows the effect of a Hanning window of length 254 samples. The same profile shape and frequency response as with Hamming window is observed. Figure 3.5 shows the effect of a Blackman window of length 254 samples on the delay profile. The delay component at t=138 vanishes, while the magnitude of delay component at t=143 has been reduced. The Blackman window therefore has the greatest effect in removing the noise.

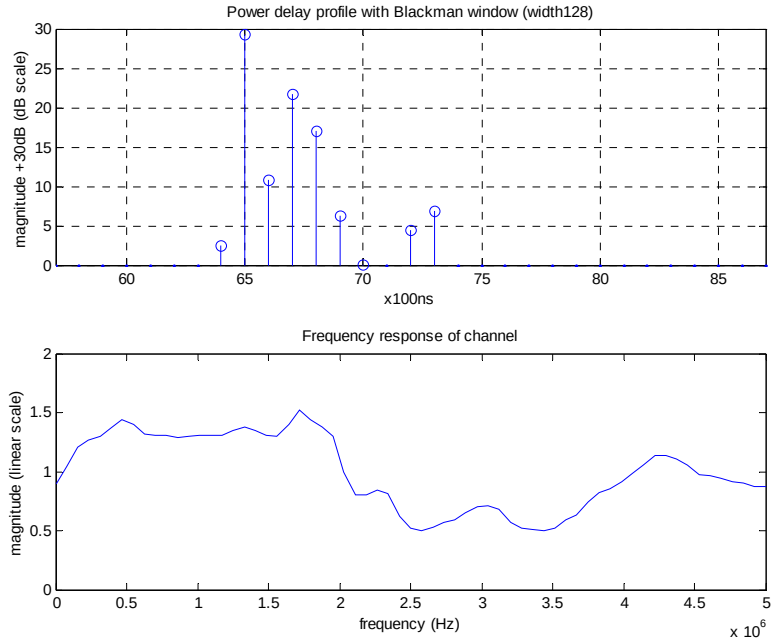

Figure 3.6 Power Delay Profile and frequency response with a Blackman Window (length 128 samples)

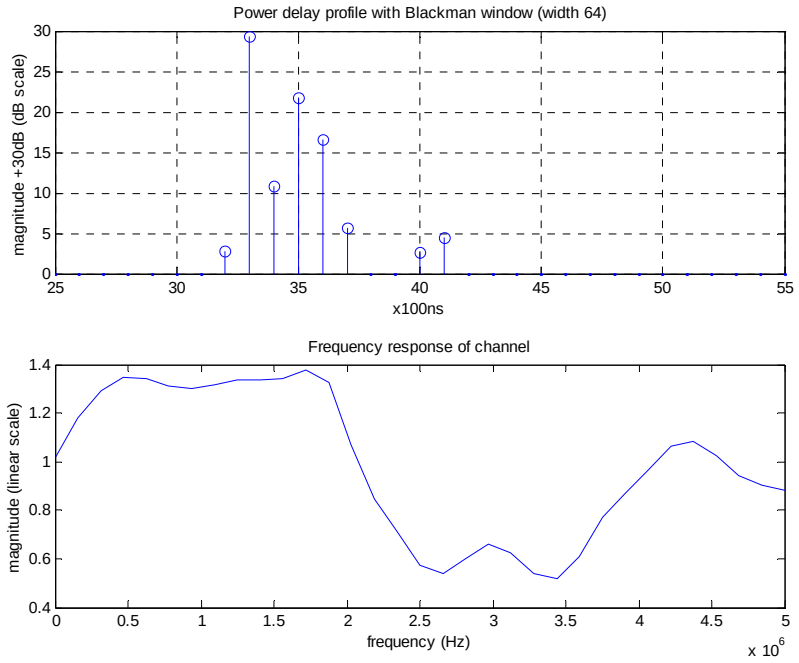

Figure 3.7 Power Delay Profile and frequency response with a Blackman Window (length 64 samples)

Figure 3.6 and 3.7 shows the effects of the window size on the power delay profile and frequency response of the channel. Because of the reduction in the size of the DFT tranformation in Figure 3.6, the centre of the main peak response is shifted to t=65. Figure 3.6 shows that using a window length of 128 samples, the delay profile shape is preserved and that the original delay component at t=143 of Figure 3.5 (which should now be at t=80 after time-shifting) has vanished. This will undoubtedly reduce the RMS delay spread value of the profile. Figure 3.7 shows the effect of further reducing the window size. Here the delay profile shape is slightly altered, particularly the last two remaining delay components are now substantially smaller than in the previous profiles. The effect is most obvious in the frequency response plot, where all the minute details have been smoothed out. Thus it can be concluded that reducing the window length has an effect of frequency averaging. In order to provide good noise reduction and at the same time preserving the delay profile shape, the window length used in subsequent calculations of RMS delay spread is set to 128 samples.

3.2 Noise Threshold dependency of RMS delay spread

The usual way to cancel the effect of noise in the power delay profile is by setting to zero the values of the average power delay profile lying below a defined noise threshold [2]. However, the noise level depends on the performance of the channel sounder and on the received power [6]. In our case, the noise floor is also dependent on the post-processing method, i.e. the choice of window function and window length. In order to investigate the effect of varying the threshold level on the sensitivity of the RMS delay spread, the threshold level was increased in steps of 1dB starting from the minimum value in the delay profile up to a value 20dB below the maximum value in the delay profile. Note that 10 delay profiles are averaged for each measurements location when evaluating the RMS delay spread.

Figure 3.8 to 3.10 shows the effect of applying different noise threshold cut-off levels on the RMS delay spread value for different window functions. The effect of the Hamming and the Hanning windows on the maximum RMS delay spread (corresponding to the maximum value in Figure 3.8 and 3.9 respectively) is very similar at 275ns and 262ns respectively. The Blackman window shown in Figure 3.10 has the smallest RMS delay spread, at 212ns. Note that these values correspond to measuring the delay spread down to the noise floor of the delay profile. A more sensible way is to fix the threshold value at a certain value, so that the RMS delay spread is not dependent on the choice of window function. For Figures 3.8 to 3.10, the threshold value should be 30dB, because this is where the RMS delay spread has stabilised following an initial roll-off stage as the threshold level is increased. At this threshold level, all three window function give similar RMS delay spread values, i.e. Hamming and Hanning windows are both 117ns and the Blackman window is 115ns. The author of [6] suggests that the threshold value should be set to a value larger than 20dB. For most of the delay profiles encountered in our case, the noise floor is substantially lower than 30dB, therefore the threshold value is set to 30dB for the subsequent calculations.

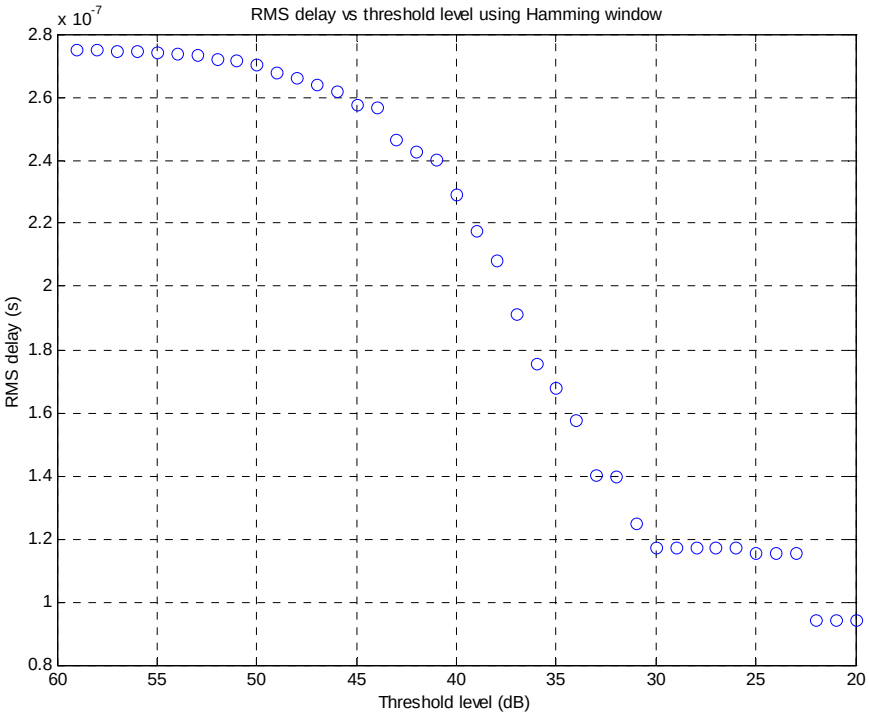

Figure 3.8 RMS delay spread vs threshold level for a Hamming window

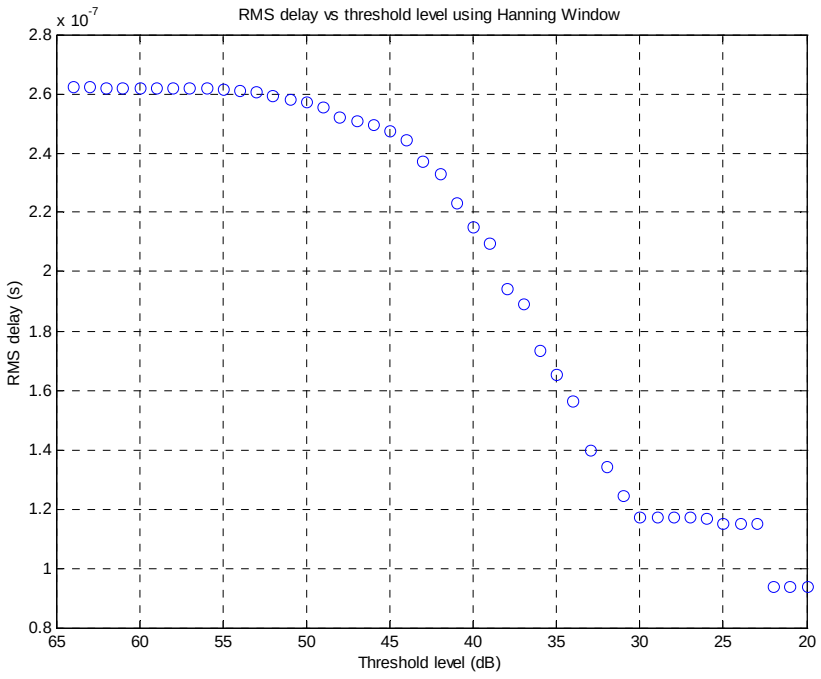

Figure 3.9 RMS delay spread vs threshold level for a Hanning window

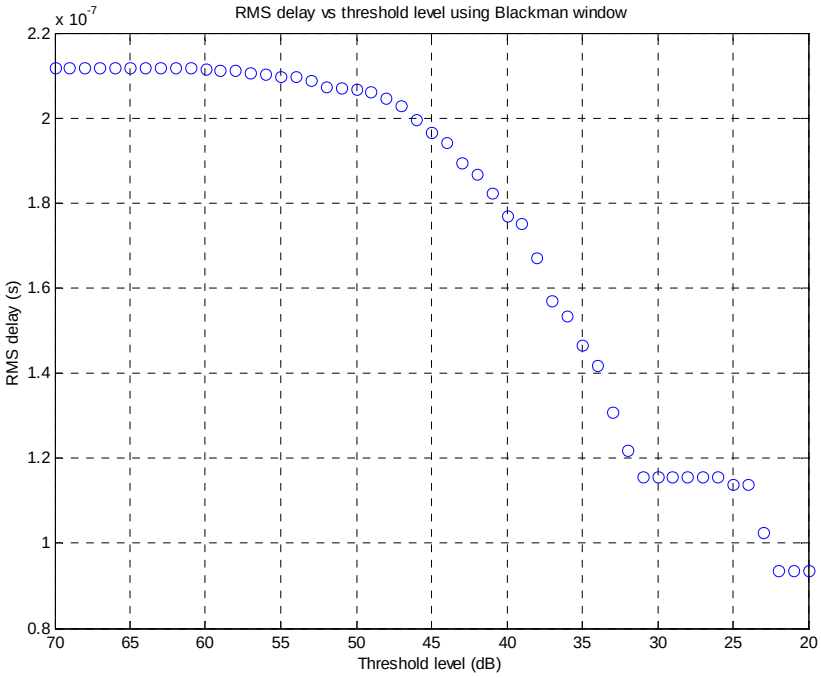

Figure 3.10 RMS delay spread vs threshold level for a Blackman window

3.3 Effect of distance, receive antenna height and excess path loss on RMS delay spread

Given that the post-processing method is fairly complete at this stage, we can now investigate the relationship between RMS delay spread and various other parameters including the distance from access point (AP) to subscriber unit (SU), subscriber unit antenna height, and path loss. The set of data studied is from some channel sounding tests conducted between 25 June 2001 and 5 July 2001 in the City of Cambridge in the United Kingdom. Further details of the experimental setup and measurement area are available in [1]. A total of 357 delay profiles collected from 17 measurement sites ranging from 0.57km to 5.4km separation are analysed.

Figure 3.11 shows the cumulative distribution of RMS delay spread of all the delay profiles collected in these tests. A Blackman window of length 128 samples is used in all subsequent analysis.

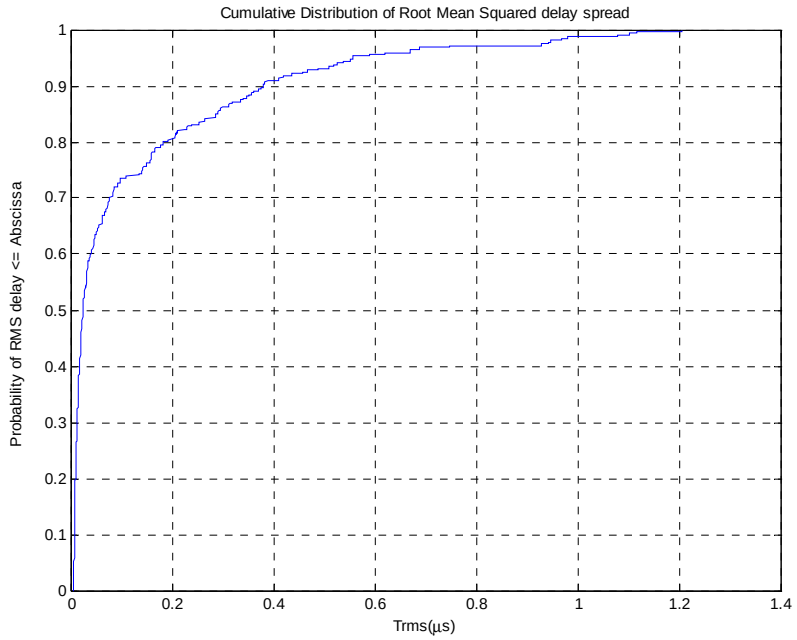

Figure 3.11 Cumulative distribution of RMS delay spread for all delay profiles

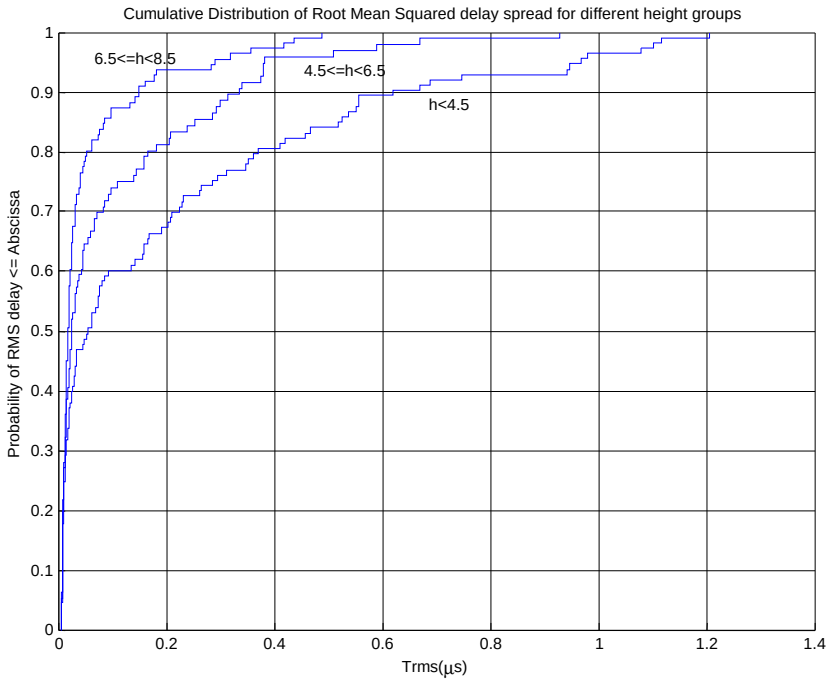

Figure 3.12 Cumulative distribution of RMS delay spread for different subscriber antenna height groups

subscriber antenna height (m)	Min (μs)	max(μs)	mean(μs)	median(μs)	std(μs)
All h	0.0057	1.21	0.123	0.0245	0.215
0.5≤h<4.5 low	0.0058	1.21	0.206	0.0557	0.297
4.5≤h<6.5 medium	0.0062	0.93	0.103	0.0251	0.163
6.5≤h<8.5 high	0.0057	0.49	0.054	0.0186	0.0925

Table 1 Statistics of RMS delay spread for different subscriber unit antenna height groups

Figure 3.12 shows the cumulative distribution of RMS delay spread for different subscriber antenna height groups and the relevant statistics are tabulated in Table 1. The heights are measured from the roof of the channel sounding vehicle (Land Rover of overall height about 2m). It is evident that RMS delay spread depends on the height of subscriber antenna. In order to further investigate the dependence of height on the RMS delay spread, a least square regression line was fitted to the logarithm of the RMS delay spread, together with the 95% confidence interval error bounds in Figure 3.13.

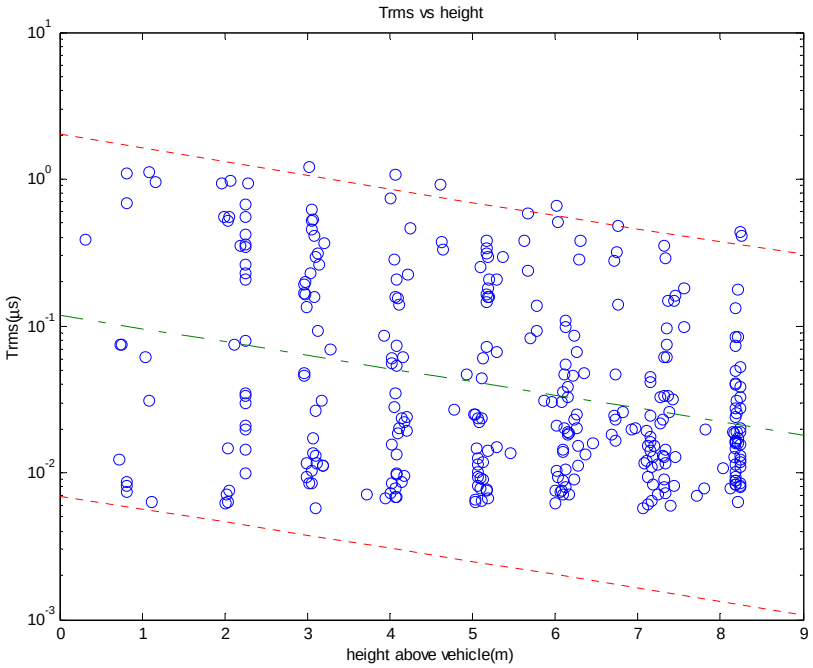

Figure 3.13 Least square regression fit of RMS delay spread against SU antenna height

The regression line is given by $\log_{10}(\text{Trms}) = -0.09h - 0.93$, where Trms is the RMS delay spread and h is the SU antenna height above the vehicle. The correlation coefficient of the regression line is -0.302, showing weak correlation (correlation coefficients close to +/-1 indicates that both parameters are related to each other). This shows that in general, RMS delay spread decreases exponentially with an increase in the SU antenna height. However our finding is not supported by [7], where the opposite is observed. It was reported in [7] that the delay spread increases slightly with higher receive antenna due to greater likelihood of a higher antenna gathering reflections from distant objects. More measurements are needed to investigate the effect of receive antenna height on the RMS delay spread.

Figure 3.14 shows a scatter plot of RMS delay spread as a function of the distance separating the AP and SU for a low SU antenna height. Figure 3.15 and 3.16 shows the RMS delay spread plotted against separation for medium and high SU antenna heights. Because of limited number of profiles studied, it is inconclusive to draw the conclusion from these scatter plots that the RMS delay spread is a function of distance. More measurements are needed to quantify the effect of antenna separation on the RMS delay spread.

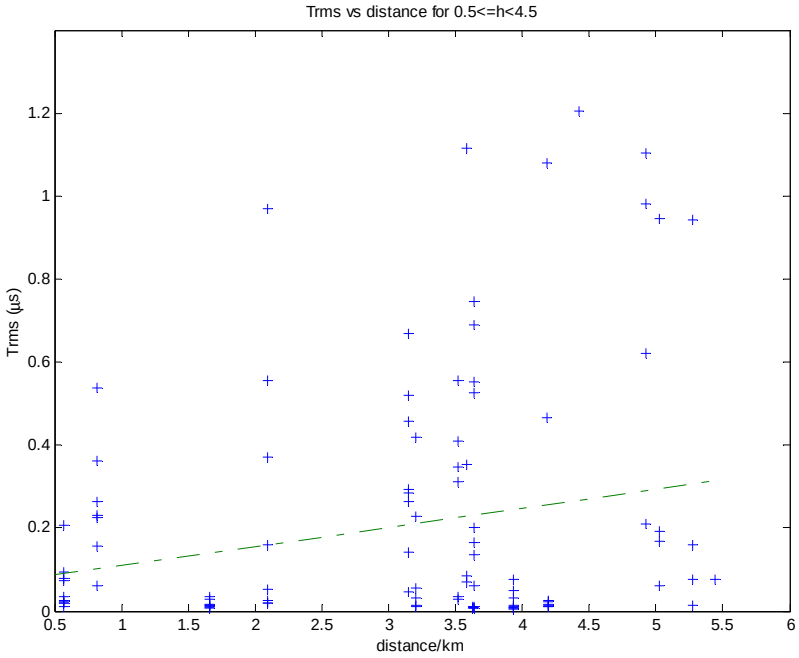

Figure 3.14 RMS delay spread against distance for low SU antenna height

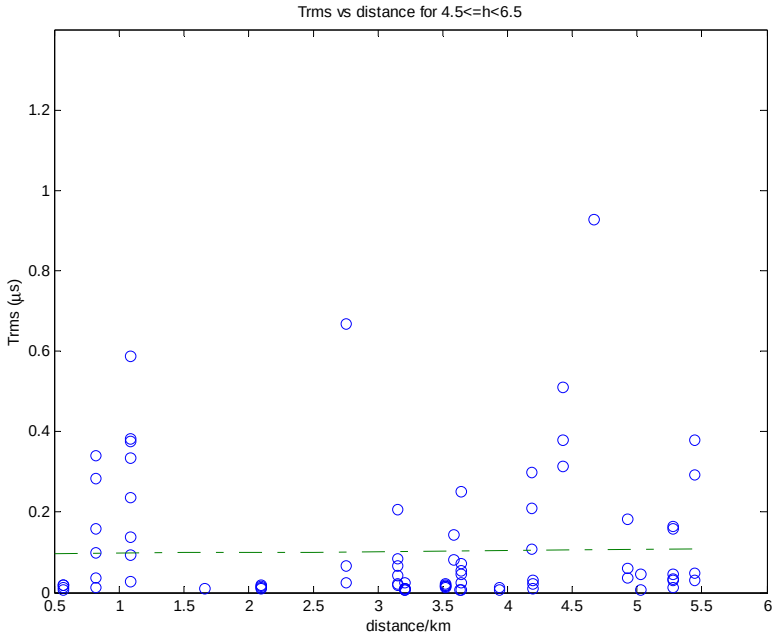

Figure 3.15 RMS delay spread against distance for medium SU antenna height

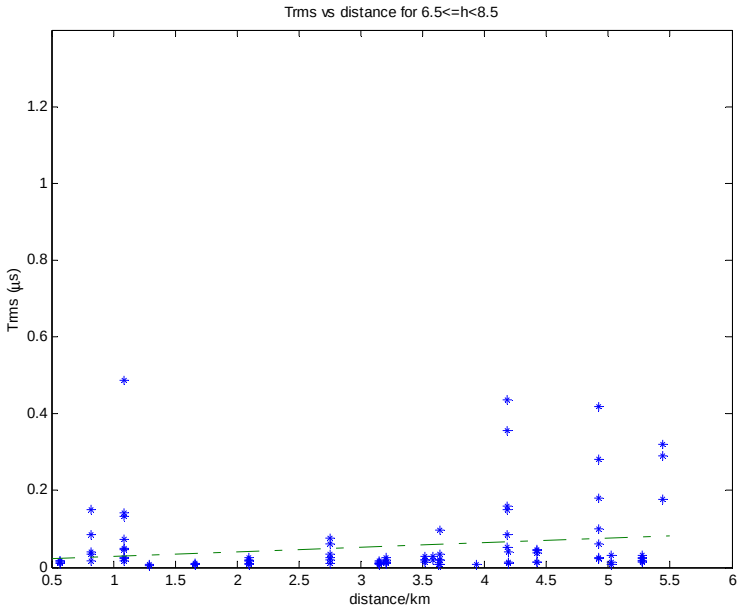

Figure 3.16 RMS delay spread against distance for high SU antenna height

Figure 3.17 shows a scatter plot of RMS delay spread plotted against excess path loss (XL), together with the least square regression fit and the 95% confidence interval error bounds. Excess path loss is defined as the path loss over and above the free space path loss. Figure 3.17 shows that delay spread is highly correlated to the excess path loss. Two regression lines are fitted, one for excess loss below 20dB, while the other is for excess losses above 20dB. The correlation coefficient of the second regression line is 0.83 (which is very close to 1) indicating that both parameters are related to each other. This regression line takes the form

$$\log_{10}(\text{Trms}) = 0.066(\text{XL}) - 3.57$$

where Trms is the RMS delay spread and XL is the excess path loss in dB. The reason for fitting two regression lines instead of one polynomial line is because when the excess path loss is low, the propagation mechanism approaches that of free space propagation. This corresponds with line-of-sight operation, hence lower multipath delay is observed in the power delay profile.

The dependence of RMS delay spread on excess path loss is also reported in [8], [9] and [10], for an omnidirectional SU antenna. This supports our finding that RMS delay spread is related to excess path loss.

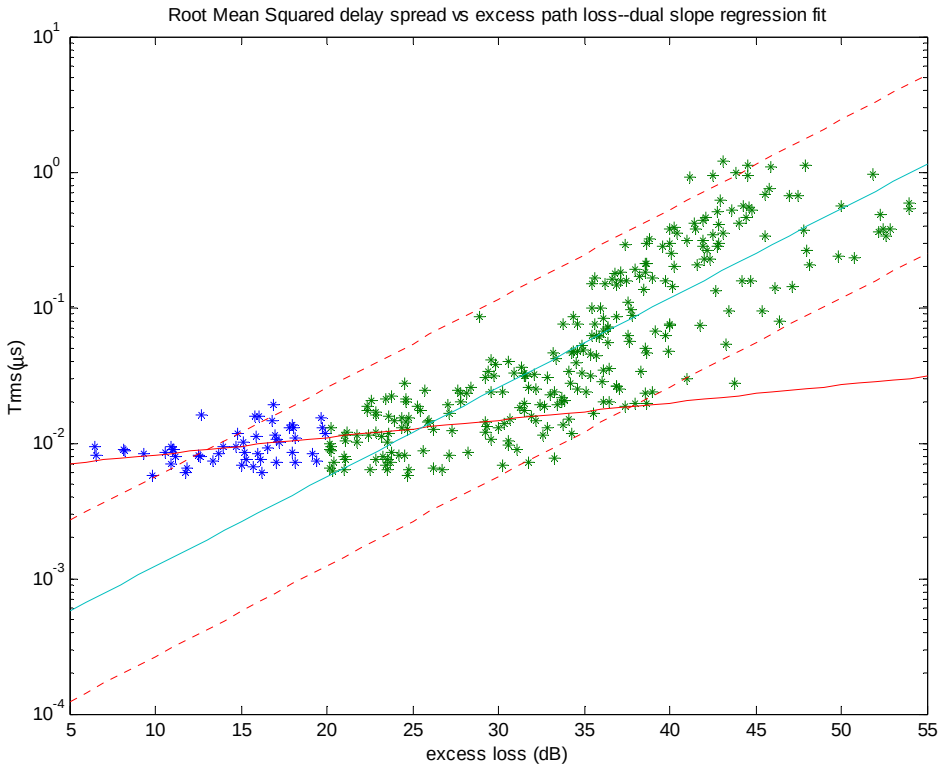

Figure 3.17 Regression plot of RMS delay spread against excess path loss.

4 Conclusions

This report shows that by using correlation methods and frequency domain processing, and by taking appropriate measures (windowing and noise threshold selection) to counter the side effects of DFT processing, the dynamic range of the channel sounding results can be improved substantially. RMS delay spread is observed to depend on excess path loss, and to a lesser extent on the SU antenna height. Further measurements are required to validate these results.

With the much-improved post-processing method, the detailed multipath structure of the radio channel can now be investigated, in order to derive an empirical Tapped-delay line model of the channel. Other factors such as the environmental (foliage and terrain) and building database (height distribution and building density distribution) will be statistically analysed and incorporated into the physical-statistical wideband channel model proposed in [1].

5 Acknowledgments

I would like to thank my supervisor Ian Wassell for his guidance and support throughout my research. I would also like to thank my industrial supervisor Steve Greaves for many helpful discussions. I would like to express my gratitude to Dave Crosby for his help on the channel sounding Matlab codes. Thanks are also due to Georgia Athanasiadou for her useful comments. I would also like to acknowledge the help of all those in Cambridge Broadband Ltd who made the channel sounding equipment. This work was generously sponsored by a Peterhouse research studentship and Cambridge Broadband Ltd.

6 Progress

Work Completed

Post-processing of preliminary measurement data (5 to 7 weeks) (completed on 6 November 2001)

- Extracted Tx-Rx range from GPS latitude/longitude format
- Written a GUI for displaying maximum likelihood (ML) channel impulse response and path loss
- Post-processed raw channel impulse response data
- Calculated RMS delay spread and plotted dependence of delay spread and path loss on receiver antenna height and Tx-Rx range

Project Plan

1 Measurement campaign (4 to 8 weeks, starting date to be agreed)

- Conduct measurement campaign in order to collect enough data for meaningful statistical analysis.
- Additional measurement campaigns will be carried out throughout the project as necessary.
- Post-process measurement results (2 weeks)

2 Semi-empirical model construction (4 weeks, starting December 2001 until January 2002)

- Relate the external parameters (including antenna height and distance) with path loss and channel impulse response
- Develop semi-empirical models (including a Tapped-delay line model) of the channel and undertake curve fitting of the measured results

3 Database extraction or site survey (8 weeks, from February 2002 to late March 2002, run in parallel with model construction phase)

- Survey height of buildings in terms of number of storeys from street to street
- Extract the mean and variance of building heights and fit to statistical distributions
- Extract building to building spacing or street width for different streets from digitised maps.
- Fit building spacing statistics into statistical distributions
- Extract orientation of streets in terms of azimuth angles, using a digitised map or a conventional street map; fit to a statistical distribution

4 Physical-statistical model construction (24 weeks April 2002 to September 2002)

- Use the knife-edge diffraction method or the GTD/UTD method to evaluate multiple half-screen diffraction, to model path loss due to diffraction over rooftops
- Use David Crosby's Random Height model to evaluate path loss, possibly extending the model to work at 3.5GHz. Evaluate excess path loss and shadow loss to model RMS delay spread.
- Evaluate wideband channel impulse response and path loss predictions based upon point-to-point ray tracing (in collaboration with Georgia Athanasiadou)
- Relate the statistical parameters to the physical model (multiple diffraction models or ray-tracing models), to form the physical-statistical model for path loss, shadow fading, fast fading (for narrowband and individual tap-gains of wideband tapped-delay line model) and delay spread
- Each models should be tested and validated with measurement results

5 Model testing and validation (6 week, October 2002 to January 2003)

- Test models against new data, fine-tune model if significant deviation is observed

6 Thesis writing (24 to 34weeks, February 2003 to September 2003)

- Allow at least 6 months to writing up thesis
- Additional refinement of models may take up to an additional 10 weeks

7 References

[1] Hong C. L. , “Improved Propagation Modelling of Broadband Fixed Wireless Access” Draft First Year Report 10 Sept 2001. LCE, Department of Engineering, University of Cambridge.

[2] P. J. Cullen, P. C. Fannin, A. Molina, “Wide-band Measurements and Analysis Techniques for the Mobile Radio Channel”, *IEEE Trans. On Vehicular Technology,* Vol. 42, No. 4, November 1993, pp. 589-602.

[3] P. A. Bello, “Characterization of Randomly Time-Variant Linear Channels”, *IEEE Trans on Communication Systems*, Vol CS-11, No. 1, March 1963, pp. 360-393

[4] Proakis, J. G., “Digital Communications”, Third Edition, 1995, McGraw-Hill Book Company, New York pp68-72

[5] Paul A. Lynn, Wolfgang Fuerst, “Introductory Digital Signal Processing with Computer Applications”, Wiley 2nd edition 1997 pp255-261.

[6] Rossi J.P. “Influence of Measurement Conditions on the Evaluation of some radio channel parameters.”, *IEEE Trans. On Vehicular Technology,* Vol. 48, No. 4, July 1999, pp1304-1316

[7] Porter J. W., Thweatt J. A. , “Microwave Propagation Characteristics in the MMDS Frequency band”, *International Conference on Communications ICC 2000 Conference Proceedings,* pp1578-1582.

[8] Greenstein L. J., Erceg V. , Yeh Y. S., Clark M. V. “A new path-gain/delay spread propagation model for digital cellular channels”, *IEEE Trans. On Vehicular Technology,* Vol. 46, No.2, May 1997, pp477-485

[9] Sousa E. S., Jovanovic V. M, Daigneault C., “Delay spread measurements for the digital cellular channel in Toronto”, *IEEE Trans. On Vehicular Technology,* Vol 43, No. 4, November 1994, pp837-846.

[10] Feurstein M. J., Blackard, K. L., Rappaport T. S., Seidel S. Y., Xia H. H., “Path loss, delay spread, and outage models as functions of antenna height for microcellular system design”, *IEEE Trans. On Vehicular Technology,* Vol. 43, No. 3, August 1994, pp486-498.